

Experimental behaviour of elliptical hollow section welded X- and T- joints

T. Haque

University of Toronto, Toronto, Ontario, Canada

ABSTRACT: Elliptical hollow sections (EHS) are the newest steel shape to emerge in the structural tube industry. Having already been implemented into structures without appropriate design guidelines, the need to establish safe, yet economical, design equations and/or procedures is imperative. EHS have often been used for truss applications, which require welded joints. This paper describes the research that experimentally investigated the static behaviour of 12 X- and T- EHS-to-EHS welded joints and examines the validity or adaptability of existing design equations by implementing different cross-sectional shape conversion approaches.

1 INTRODUCTION

Elliptical hollow sections (EHS) are the newest steel shape to emerge in the structural tube industry. Their unique shape has provided a modern aesthetically appealing look to architectural and structural features. The implementation of EHS can be found in various structures around the world, but it has been done so without appropriate design guidelines. To ensure the safe, yet economical, implementation of EHS into structures, it is imperative that design equations and/or procedures be established.

Architecturally, hollow structural sections (HSS) are often used in trusses because they are aesthetically appealing and represent an overall economic benefit. Structurally, this application typically requires welded branch-to-chord joints for practical and aesthetic reasons. EHS, like other HSS, have been used in truss systems, such as the example of the glass facade of the AXA Building in Paris, France (Bortolotti et al., 2003).

Research on EHS has focused on cross-sectional classification, compressive and bending strength of EHS, etc., but few studies have focused on EHS joints. Willibald et al. (2006) studied EHS through- and branch-plate joints and Martinez-Saucedo et al. (2008) studied EHS end-joints, but neither of these looked at EHS-to-EHS joints. Existing studies on EHS-to-EHS joints have included the investigation of an EHS truss joint of the AXA building by Bortolotti et al. (2003) and finite element analyses of EHS X-joints by Pietrapertosa and Jaspert (2003)

and Choo et al. (2003). Despite previous studies, the database of EHS-to-EHS experimentally tested joints remains small. It remains insufficient to perform the finite element modelling and parametric analyses necessary to develop suitable design equations. In order to establish joint design guidelines, the database of experimentally tested EHS-to-EHS welded joints needs to be expanded.

2 EXPERIMENTAL PROGRAMME

The purpose of this research programme is to expand the database of experimentally tested EHS-to-EHS joints. The first objective is to further understand the behaviour of these EHS joints. With this understanding, finite element models can be created to corroborate the experimental results. These models can then be used for parametric analyses to develop the necessary design equations. The second objective is to compare these experimental values with existing HSS design equations. By using cross-sectional shape conversion approaches, the results from this experimental programme will be used to examine the validity or adaptability of these other HSS equations for EHS use. This experimental programme includes 12 large-scale EHS-to-EHS welded joint specimens tested under quasi-static loading at the University of Toronto.

2.1 Specimens

All specimens were fabricated using EHS $220 \times 110 \times 6$ ($H \times B \times t =$ large dimension \times small dimension \times thickness) with a steel grade of EN10210 S355J2H (CEN 2006a, 2006b). Measured geometrical properties are $H = 220$ mm, $B = 110$ mm, $t = 5.94$ mm with a cross-sectional area $A_{EHS} = 3044\text{mm}^2$. Figure 1 shows a typical EHS cross-section, labelling the key dimensions and cross-sectional regions.

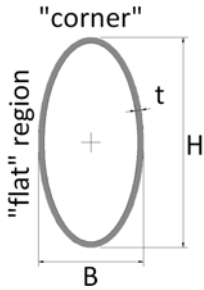


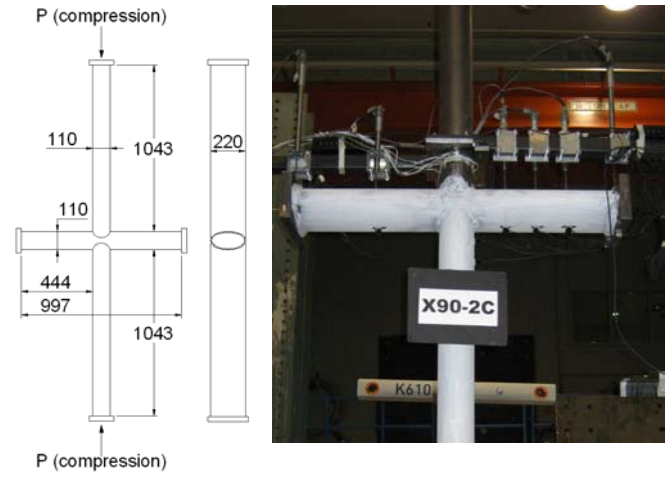
Figure 1. EHS cross-section.

The specimens were designed to have sufficient chord and branch lengths to minimize the effects that the boundary conditions could have on the joint. The joint welds were specified to have a minimum effective throat of $1.1t$. All joints were tested by applying a quasi-static axial load to the branch (or branches) using a MTS 2700kN-capacity Universal Testing Machine. Compression tested joints were laterally braced against out-of-plane buckling. Table 1 lists the specimen details of the 12 EHS joints tested. Figure 1 shows an example of an X-joint at 90° , Figure 2 shows an example of a T-joint at 90° , and Figure 3 shows an example of a X-joint at 45° .

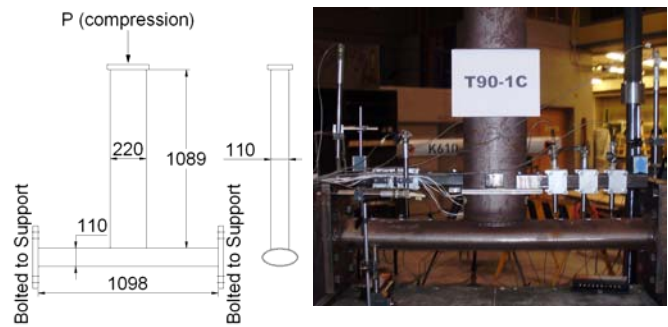
Table 1. Experimental programme and specimen chord and branch(es) measurements.

Test #	Designation	Chord	L/b_0	Branch(es)
		Length (L)		Length
		mm		mm
1	X90-1T	2198	9.99	1089
2	X90-2T	994	4.52	1045
3	X90-3T	1016	9.24	989
4	X90-1C	2193	9.97	1089
5	X90-2C	997	4.53	1043
6	X90-3C	1016	9.24	989
7	X45-1C	2264	10.29	890/1110*
8	X45-2C	963	4.38	987/1097*
9	X45-3C	1326	12.05	879/1099*
10	T90-1C	1098	4.99	1089
11	T90-2C	1098	4.99	1042
12	T90-3C	1100	10.00	1032

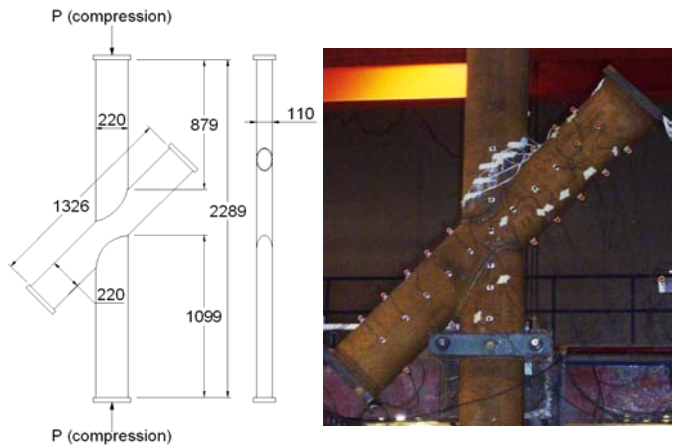
*minimum/maximum distance to chord top or bottom



(a) Dimensions (b) Experimental set-up
Figure 1. Specimen X90-2C.



(a) Dimensions (b) Experimental set-up
Figure 2. Specimen T90-1C.



(a) Dimensions (b) Experimental set-up
Figure 3. Specimen X45-3C.

In Table 1, under the “Designation” heading, the first character is a T or X and represents either a T- or X-joint. T-joints consist of one branch and X-joints consist of two branches. The first number is 90 or 45 and represents the joint branch-to-chord angle in degrees. The second number is a 1, 2 or 3 and represents the joint orientation type. The last character is a T or C and indicates whether the joint was loaded in branch tension or compression. Chord length is the length from chord end-to-end, not including the end plates, and branch length is the

length from branch end to chord top or bottom, not including the end plate.

There are 4 joint orientation types attributed to Choo et al. (2006), but only 3 types were physically possible for this experimental programme: types 1, 2, and 3. Figure 4 shows the orientations of each type. Since the EHS branches and chords were the same cross-section for this experimental programme, joint orientation types resulted in certain measurements and parameters being the same regardless of angle or loading. These constants can be found in Table 2. The headings b_0 and h_0 represent the chord width (transverse to the length of the chord) and height, and the headings b_1 and h_1 represent the branch width (transverse to the length of the chord) and height. $\beta = b_1/b_0$ and $\eta = h_1/b_0$.

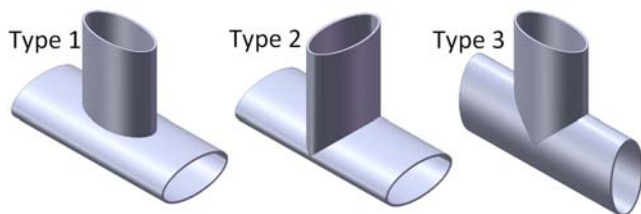


Figure 4. Types 1, 2 and 3 branch-to-chord orientations

Table 2: Constant measurements and parameters for joint orientations types 1, 2, and 3 tested

Type	b_0	h_0	b_1	h_1	β	η
	mm	mm	mm	mm		
1	220	110	110	220	0.5	1.0
2	220	110	220	110	1.0	0.5
3	110	220	110	220	1.0	2.0

2.2 Instrumentation

To measure the joint displacement, chord deformation profile and stress profile near the joint, three sets of instrumentation were used. The first set includes LVDTs (linear variable displacement transducers) mounted along the chord top and at the joint to measure the chord deformation profile and joint displacement (seen in Figures 1b and 2b). The capability of the LVDTs, however, was limited. The LVDTs could not be properly mounted for the 45° specimens, and the joint displacement LVDT would often lead to poor readings due to out-of-plane local buckling and rotation. This led to the second set of instrumentation, which includes a K610 remote 3D optical scanner with LEDs (light emitting diodes) (seen in Figure 3b). For the 45° specimens, or where there was out-of-plane movement at the joint leading to poor LVDT readings, the optical scanner system was used to measure joint displacement and could also be used to measure the chord deformation profiles, out-of-plane displacements, and rotations. The third set of instrumentation includes strain gauges positioned around half the top branch perimeter, near the welds, to measure the stress profile.

The strain gauge data will subsequently be used for the finite element model validation.

3 RESULTS

The experimental results include determining material properties, load-joint displacement curves, failure modes and chord deformation profile, which are described below.

3.1 Material property tests

To determine the EHS material properties, 3 tensile coupon (TC) tests were performed. Each coupon was taken from a different part of the same cross-section, two from along the “flat” region and one from the “corner” of the EHS (see Figure 1). The average results from those tests are found in Table 3 where f_y is the yield stress, f_u is the ultimate stress and E is Young’s modulus.

A stub column test was performed according to Galambos (1995) to corroborate the results obtained from the tensile coupon tests. From the stub column test, $E = 208.1\text{GPa}$, approximately the same value determined by the tensile coupon tests. The stub column reached an ultimate stress of 430MPa. This is much lower than the ultimate stress determined from the tensile coupon tests as the stub column underwent local buckling when it reached its maximum load (Figure 5) rather than extensive strain hardening and necking.

Table 3. EHS material properties from tensile coupon tests.

Coupon	f_y	f_u	E
	MPa	MPa	GPa
TC-1	408.0	522.6	211.4
TC-2	399.5	516.0	201.5
TC-3	401.5	511.6	217.3
Average	401.5	516.7	210.1



Figure 5. Local buckling of EHS cross-section from stub-column test.

3.2 Load-joint displacement curves and failure modes

The load-joint displacement curves for the 12 joints were determined, where the joint displacement refers to the measured displacement the branch undergoes perpendicular to the chord centreline. Table 4 lists the capacity of the joint at the ultimate load and the 3% deformation limit. The 3% deformation limit is the joint capacity when the joint displacement reaches 3% of the chord width (b_0). This limit is 6.6 mm for type 1 and 2 joints, and 3.3 mm for type 3 joints.

Under the “Load Capacity” heading, the highlighted values indicate the governing capacity. Under the “Failure Mode” heading, the acronyms mean the following: BF – branch failure, CP – chord plastification, CT – chord tear-out, GB – global buckling (overall), and SW – chord side-wall failure, and indicate the failure mode at ultimate load.

Figures 6, 8, 9, and 11 are load-joint displacement curves that provide a representative sample of the typical behaviour of the tested joints. N_1 is the joint (branch) load, Δ_1 is the joint displacement, and the subscripts “3%” and “u” indicate the 3% deformation limit and ultimate load, respectively.

Table 4. Load capacities and failure modes

Joint	Load Capacity		Failure Mode
	Ultimate	3% b_0 Limit	
	kN	kN	
X90-1T	339.1	188.0	CP; CT
X90-2T	596.8	574.5	BF; SW
X90-3T	1557.0	1188.8	BF
X90-1C	202.0	150.5	CP
X90-2C	539.7	531.5	GB
X90-3C	555.1	543.4	CP; SW
X45-1C	350.3	244.0	CP
X45-2C	627.8	618.0	CP
X45-3C	701.0	388.7	CP; SW
T90-1C	216.5	211.4	CP
T90-2C	353.0	338.2	CP; SW
T90-3C	593.8	550.6	CP; SW

3.2.1 Branch tension tests

The capacity of all tension tested joints was governed by the 3% deformation limit. The behaviour of the type 1 and type 2 tests, X90-1T and X90-2T, was similar: as the load increased, the chord of the joint increasingly “circularized” until chord tearing was prevalent causing a drop in load carried. Figure 6 shows the load-joint displacement curve for X90-2T, a typical representation of type 1 or 2 tension tested joints and Figure 7 shows X90-2T at ultimate failure. The behaviour of the type 3 test, X90-3T, was different. It experienced smaller joint-displacements and its failure mode was

governed by branch failure. Figure 8 shows the load-joint displacement curve for X90-3T where the second increase in load capacity is attributed to strain-hardening of the branch members and the final load drop is due to the branch rupturing.

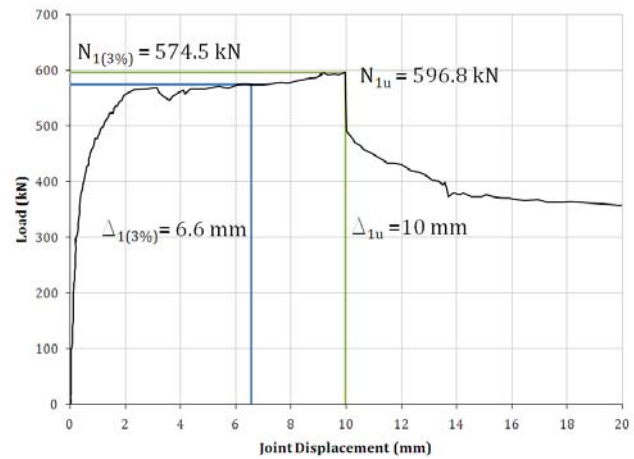


Figure 6. X90-2T load-joint displacement curve; typical curve for type 1 and 2 tension-tested joints.



Figure 7. X90-2T failure mode showing an example of chord tearing for a tension test.

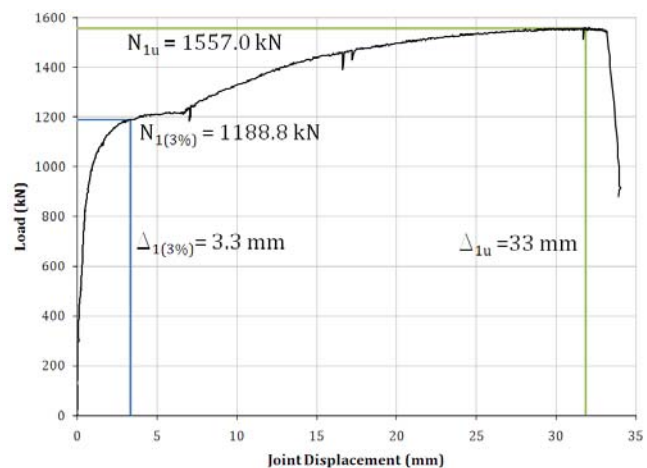


Figure 8. X90-3T load-joint displacement curve; typical curve for type 3 tension-tested joints.

3.2.2 Branch compression tests

X-joints at 45° have higher capacities than their 90° T- or X- counterparts. Generally, the capacities of type 1 compression tested joints are governed by the 3% deformation limit, and the capacities of type 2 and 3 compression tested joints are governed by the ultimate limit. The only case for which this is not the case is for the type 1 T-joint, T90-1C; however, the ultimate and the 3% limit nearly coincide (both occurring with a joint deformation of approximately 6.6mm).

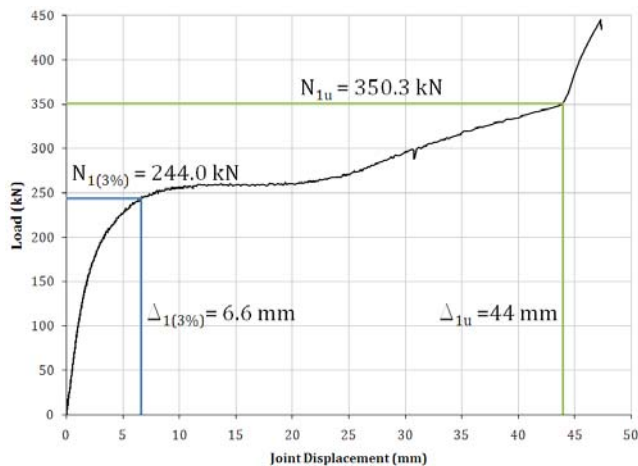


Figure 9. X45-1C load-joint displacement curve; typical curve for type 1 compression-tested joints.



Figure 10. X45-1C chord plastification failure as the chord flattens at the joint; typical failure for type 1 joints.

Typically, type 1 ($\beta = 0.5$) joints increasingly flatten to two plates as the load increases. The capacity of the joint plateaus, but due to the tension stiffening of the top and/or bottom of the chord as the branches flatten the chord, the capacity of the joint increases. Figure 9 shows the load-joint displacement curve for X45-1C, a typical curve for type 1 joints and Figure 10 shows X45-1C at failure, the typical failure mode for type 1 joints.

For the type 2 and 3 joints ($\beta = 1.0$), chord side-wall failure was prevalent. The buckling of the

chord sidewalls led to the drop in load capacity. Figure 11 shows the load-joint displacement curve for T90-3C, a typical curve for type 2 and 3 joints, and Figure 12 shows the T90-3C side-wall failure.

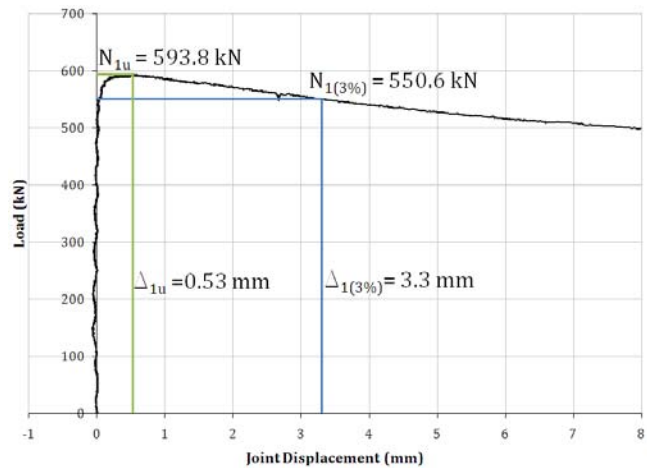


Figure 11. T90-3C load-joint displacement curve; typical curve for type 2 or 3 compression-tested joints.

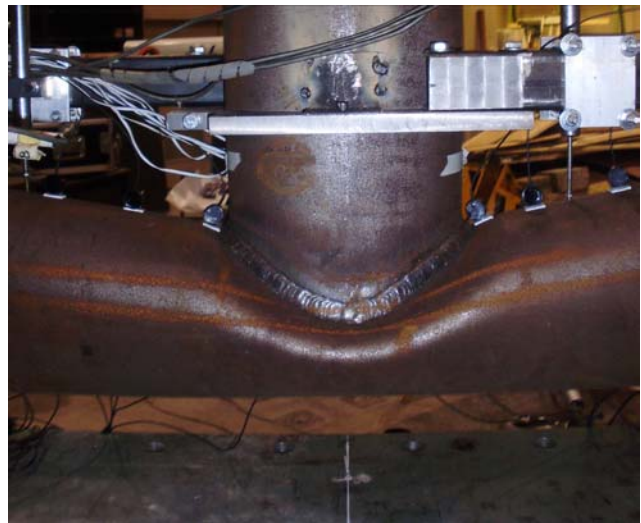
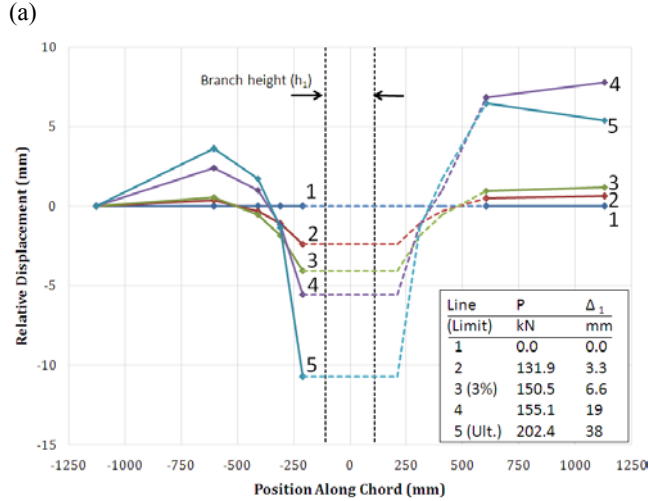


Figure 12. T90-3C side-wall failure; typical failure for type 2 and 3 joints.

3.2.3 Chord deformation profiles

LVDTs and/or LEDs were placed along the top of the chord to measure the chord deformation profile of the connecting face. As the MTS 2700kN-capacity machine displacement increased, the displacement of the joint relative to the overall chord deformations became more prominent. Figure 13 shows the chord deformation profile for X90-1C at various joint deformations (Δ_1) and loads (P), using the leftmost LVDT as the point of reference. This figure represents a typical chord deformation profile of the connecting face for a 90° compression-tested joint. The displacement points are the locations of the LVDT or LED and the dashed lines indicate assumed deformations based on the symmetry of the specimen. Linear interpolation was used for values between the displacement points.

For the branch tension tests, the chord near the joint experiences positive relative displacements (compared to the compression-loaded joint which undergoes negative relative displacement).



(b) Figure 13a (above). X90-1C location of LVDTs (not including ends) and indentation of the chord at the joint. Figure 13b (below). X90-1C chord deformation profile of top connecting face.

4 JOINT STRENGTH PREDICTIONS

Two methods of converting an EHS into an equivalent shape for which design equations already exist have been proposed by Zhao and Packer (2009) and Ruiz-Teran and Gardner (2008), for equivalent RHS and equivalent CHS respectively. These methods are used in this paper to convert each EHS joint into an equivalent RHS or EHS joint, in order to use the CIDECT Design Guides 1 and 3.

4.1 Equivalent RHS method

The procedure to convert the EHS chord into an equivalent RHS is described here. To maintain the physical parameter $\beta = b_1/b_0$, the chord width (b_0) was kept constant, regardless of joint orientation (type 1, 2, or 3). By setting the EHS chord width, area and thickness the same in the equivalent RHS and neglecting corner radii, an equivalent RHS chord height ($h_{0,eq}$) was calculated. (This is very similar to a procedure described by Zhao and Packer

(2009) for treating EHS under axial compression). For the EHS used in all test specimens, the measured cross-sectional area $A_{EHS} = 3044\text{mm}^2$. Equation 1 summarizes the procedure to calculate $h_{0,eq}$.

$$h_{0,eq} = \frac{A_{EHS} - 2tb_0 + 4t^2}{2t} \quad (1)$$

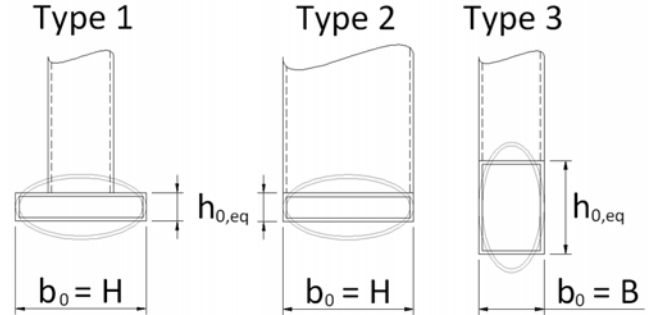


Figure 14. Equivalent chord height using the equivalent RHS method.

For type 1 and 2 orientations, the width of the chord is H, so the equivalent RHS height $h_{0,eq} = 48.1\text{mm}$. For Type 3 orientations, the width of the chord is B, so the equivalent RHS height $h_{0,eq} = 158.1\text{mm}$ (see Figure 14). These new values were used to predict the joint capacities given in Table 5.

Using Table 4.1 from CIDECT Design Guide No. 3 (Packer et al., 2009) and by converting the chord into an equivalent RHS and the branch into an RHS of outer dimensions $h_1 \times b_1$, joint capacity predictions were made and the governing resistances are summarized in Table 5 and compared with the actual joint capacity.

The Q_f factor found in the chord face plastification and chord side wall failure CIDECT design equations becomes less than 1.0 for the T-joints. This is because the T-joints had fixed-end restraints causing moments to develop in the chord at the joint (M_0). M_0 is calculated according to equation 2:

$$M_0 = \frac{N_{1f}}{8}(L - h_1) \quad (2)$$

where N_{1f} is the governing load capacity of the joint (Table 4), L is the chord length (Table 1) and h_1 is the branch height (Table 2). To calculate the plastic moment capacity of the chord ($M_{pl,0}$), the real plastic section modulus (Z) of the EHS was used; for major-axis bending (type 3 joint), $Z = 179.0 \times 10^3 \text{mm}^3$ and for minor-axis bending (type 1 and 2 joints), $Z = 109.7 \times 10^3 \text{mm}^3$.

In order to calculate the chord side-wall failure limit state, the limiting stress of the material has an effect in the f_k term. For tension, $f_k = f_{y0} = 402\text{MPa}$,

but for compression, χ , a reduction factor for column buckling, becomes relevant. The following describes the procedure used to calculate χ . The slenderness parameter was calculated using the equation given in Table 4.1 of CIDECT Design Guide No. 3 (Packer et al., 2009), normalized using Euler's slenderness parameter and entered into the Canadian S16-09 (CSA, 2009) column flexural buckling formula which uses:

$$\chi = (1 + \lambda^{2n})^{-1/n} \quad (3)$$

where λ is the normalized slenderness parameter, and $n = 2.24$, the value stipulated for hot-formed hollow sections.

The governing resistance formula was chord face plastification for type 1 joints and chord sidewall failure for type 2 and 3 joints. The resistance formula generally captured the actual failure mode, except for X90-3T, where failure occurred by the yielding of the branch.

4.2 Equivalent CHS method

The procedure to convert the EHS chord into an equivalent CHS is described here. Using equations 4 and 5 ($H = 220.0\text{mm}$, $B = 110.0\text{mm}$, and $t = 5.94\text{mm}$), advocated by Ruiz-Teran and Gardner (2008) for treating EHS under axial compression and bending, $d_0 = D_{e,CHS} = 382.1\text{ mm}$. This equivalent diameter was used to predict the joint capacity. In order to maintain the physical parameter β , an equivalent branch diameter (d_1) was calculated according to equation 6.

$$f = 1 - 2.3 \left(\frac{t}{H} \right)^{0.6} \quad (4)$$

$$d_0 = D_{e,CHS} = H \left[1 + f \left(\frac{H}{B} - 1 \right) \right] \quad (5)$$

$$d_1 = \beta \times d_0 \quad (6)$$

Using Table 4.1 from CIDECT Design Guide No. 1 (Wardenier et al., 2008), and by converting the EHS chord and branches into equivalent CHS, joint capacity predictions were made and are summarized in Table 5. The procedure to determine Q_f for the T-joints is the same as the equivalent RHS method.

Using the CHS design equations, the governing failure mode was chord plastification for all joints. This EHS to CHS conversion method, originating from local buckling studies of EHS under normal stress, is a very dubious application for joint behaviour, and has a very large scatter too. The failure modes are not necessarily captured by using these design formulae.

4.3 Summary of predictions

Table 5 summarizes the predicted capacities using the two methods described above, and the ratio of the actual capacities to the predicted capacities. Figure 15 shows the comparison of the two methods for each of the 12 tests. From Figure 15, one can see that the equivalent RHS method shows a smaller scatter and ratios closer to 1.0, in comparison to the equivalent CHS method. However, Table 5 and Figure 15 show that these methods still have problems catering to the T-joints. Table 5 includes the mean and COV excluding the T-joint predictions to demonstrate this problem.

Table 5 : Joint predictions using existing design equations and EHS shape conversion

Joint	Actual Capacity kN	Predicted Capacity kN		Actual/Predicted Ratio	
		RHS**	CHS**	RHS**	CHS**
X90-1T	188.0	137.0	143.23	1.373	1.313
X90-2T	574.5	667.2	413.79	0.861	1.388
X90-3T	1188.8	1192.5	413.79	0.997	2.873
X90-1C	150.5	137.0	143.23	1.099	1.051
X90-2C	539.7	532.8	413.79	1.013	1.304
X90-3C	555.1	571.7	413.79	0.971	1.342
X45-1C	244.0	226.9	202.56	1.075	1.205
X45-2C	627.8	705.0	585.19	0.891	1.073
X45-3C	701.0	600.1	585.19	1.168	1.198
T90-1C	216.5	104.5	155.0	2.072*	1.397*
T90-2C	353.0	426.5	236.2	0.828*	1.495*
T90-3C	593.8	563.1	357.6	1.054*	1.661*
Mean (all 12 tests)				1.117	1.441
COV (all 12 tests)				0.300	0.334
Mean (excluding T-joints)*				1.050*	1.416*
COV (excluding T-joints)*				0.148*	0.394*

**RHS and CHS refer to the equivalent RHS and equivalent CHS methods, respectively.

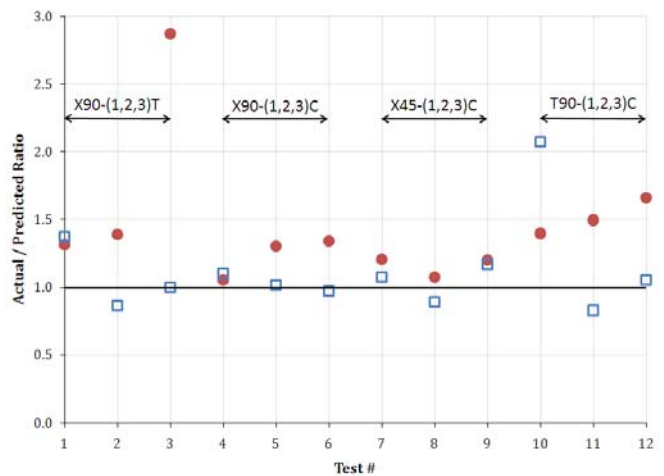


Figure 15. Actual / predicted capacity ratios of equivalent CHS (filled circles) and RHS methods (hollow squares) for 12 joints.

5 CONCLUSION

This paper describes the behaviour of various EHS-to-EHS welded X- and T-joints. The experimental programme consisted of 12 large-scale EHS-to-EHS welded joints under quasi-static loading in order to expand the database of experimentally tested EHS joints.

The results generally showed that tension-tested joints and type 1 compression-tested joints were governed by the 3% deformation limit, but type 2 and 3 compression-tested joints were governed by the ultimate load. Also, joints at 45° generally had higher joint-capacities (in terms of branch loads) than their 90° counterparts and chord deformations remained locally around the joint.

Two EHS conversion methods were examined to determine the validity of existing RHS and CHS joint design equations for EHS use. By converting the EHS chord and branches into equivalent RHS or CHS, it was found that the equivalent RHS method captures the failure mode better, overall makes better predictions and has less scatter. Further conversion methods may need to be explored to better predict the capacity of T-joints.

It is recommended that more experiments be performed to expand the database of experimentally tested EHS joints to further understand the effects of various parameters. It is also recommended that finite element models be created and validated against the results obtained from this experimental programme. Once those finite element models have been validated, parametric numerical analyses should be performed to develop suitable design equations for EHS-to-EHS joints.

6 ACKNOWLEDGEMENTS

The author gratefully acknowledges the guidance of Professor Jeffrey A. Packer and assistance from the structural laboratory staff at the University of Toronto. Financial support for this research was provided by the Natural Sciences and Engineering Research Council of Canada (NSERC) and the Steel Structures Education Foundation (SSEF). Fabrication services were generously donated by Walters Inc. (Ontario).

7 REFERENCES

Bortolotti, E., Jaspert, J. P., Pietrapertosa, C., Nicaud, G., Petitjean, P., and Grimault, J. P. 2003. Testing and modelling of welded joints between elliptical hollow sections. *10th International Symposium on Tubular Structures; Proc. Madrid, Spain*: 259-264.

CEN 2006a. Hot finished structural hollow sections of non-alloy and fine grain steels - Part 1: Tolerances, dimensions

and sectional properties, *EN10210-1(en)*. Brussels, Belgium: European Committee for Standardization.

CEN 2006b. Hot finished structural hollow sections of non-alloy and fine grain steels - Part 2: Tolerances, dimensions and sectional properties, *EN10210-2(en)*. Brussels, Belgium: European Committee for Standardization.

Choo, Y.S., Liang, J.X., and Lim, L.V. 2003. Static strength of elliptical hollow section X-joint under brace compression. *10th International Symposium on Tubular Structures; Proc. Madrid, Spain*: 253-258.

CSA 2009. *CSA-S16-09 Design of Steel Structures*. Mississauga, Canada: Canadian Standards Association (CSA).

Galambos, T.V. (ed.) 1995. Appendix B.3. *Guide to stability design criteria for metal structures* (5th ed.). New York, USA: John Wiley & Sons: 814-822.

Martinez-Saucedo, G., Packer, J.A., and Zhao, X.L. 2008. Static design of elliptical hollow section end connections. *Structures and Buildings* 161(SB2): 103-113.

Packer, J.A., Wardenier, J., Zhao, X.L., van der Vegte, G.J., and Kurobane, Y. 2009. *Design Guide for Rectangular Hollow Section (RHS) Joints Under Predominantly Static Loading* (2nd ed.); *Design Guide 3*. Switzerland: Comité International pour le Développement et l'Étude de la Construction Tubulaire (CIDECT).

Pietrapertosa, C. and Jaspert, J. P. 2003. Study of the behaviour of welded joints composed of elliptical hollow sections. *10th International Symposium on Tubular Structure; Proc. Madrid, Spain*: 259-256.

Ruiz-Teran, A. M. and Gardner, L. 2008. Elastic buckling of elliptical tubes. *Thin Walled Structures*, 46(11): 1308-1318.

Wardenier, J., Kurobane, Y., Packer, J.A., van der Vegte, G.J., and Zhao, X.L. 2008. *Design Guide for Circular Hollow Section (CHS) Joints Under Predominantly Static Loading* (2nd ed.); *Design Guide 1*. Switzerland: Comité International pour le Développement et l'Étude de la Construction Tubulaire (CIDECT).

Willibald, S., Packer, J.A., Voth, A., and Zhao, X., 2006. Through-plate joints to elliptical and circular hollow sections. *11th International Symposium on Tubular Structures; Proc. Toronto, Canada*: 221-228.

Zhao, X.L., and Packer, J.A. 2009. Tests and design of concrete-filled elliptical hollow section stub columns. *Thin-Walled Structures* 47(6-7): 617-628.